Foundation Fighting Blindness

Usher Syndrome 1B Landscape

Version 9/2021

The Foundation Fighting Blindness
www.FightingBlindness.org

Conditions of Use of Landscape

This document represents a broad literature review related to the titled subject matter. It summarizes data, news, and events from multiple sources, including peer-reviewed articles, conference abstracts, press releases, and Web-based sources. It does not represent and is not intended to represent a comprehensive collection of all work, whether research, clinical, or editorial on the titled subject matter. The content therein should be used to gain broad understanding on the titled subject matter, to frame thoughts and ideas, and to guide additional literature reviews. Unless otherwise noted, sources are peer-reviewed articles, which are considered to be of greater evidentiary/scientific value. We encourage readers to consider the source of information when reviewing this document. The content is subject to correction, updates, or clarification.

Statement of Originality

No claim is made that all text and/or figures in this document are original to the Foundation. When appropriate for accuracy, text or figures from original publications have been copied verbatim or with light editing. In most cases this is indicated in the text, and in most cases the sources are acknowledged. **It cannot be assumed that all such instances are marked.**

Copyright

This document is copyright subject to the comments of originality made above.

Table of Contents

Usher Syndrome Overview

Usher syndrome (USH) is a genetic disorder that follows an autosomal recessive inheritance. It is the most frequent cause of deaf-blindness, estimated to account for more than 50% of cases, as well as an estimated 5% of all congenital deafness cases and 18% of all retinitis pigmentosa (RP) cases. Usher syndrome traditionally is classified into 3 clinical types based on age of onset, severity and progression of symptoms, and the presence or absence of vestibular dysfunction. Usher syndrome type 1 (USH1) generally is the most severe type, USH type 2 (USH2) is the most frequent, and USH type 3 (USH3) is the rarest. Some individuals exhibit symptoms that do not readily fit into these 3 types and are classified as having atypical USH. The USH types are further subdivided (eg, USH1B) based on the disease-causing gene. However, the genotype-phenotype correlation in USH is not entirely exact, with some individuals harboring genetic variants associated with one USH type but exhibiting symptoms associated with another. (Ferrari et al, 2011; Millán et al, 2011; Fuster-Garcia et al, 2021; Toms et al, 2020)

Genes and Variants

The gene associated with USH1B, *MYO7A* (**Table 1**), was the first gene to be linked to USH, identified in 1995. Pathogenic variants of this gene are estimated to comprise 29%-50% (with some estimates of up to 70%) of USH1 cases, making it the most prevalent USH1 gene. It is the second most prevalent mutated gene in all USH cases (21% based on a 2019 study of 684 individuals with dual vision and hearing loss). In addition to USH1B, mutations in *MYO7A* can result in non-syndromic autosomal recessive and autosomal dominant hearing loss. Genetic mapping in mice has revealed a genetic network of 40 other genes with expression that is highly correlated with and may be functionally related to *MYO7A*, among which are several genes linked to retinal diseases and deafness (**Figure 1**). (Fuster-Garcia et al, 2021; Koenekoop et al, 2020; Jaijo et al, 2006; Jouret et al, 2019; French et al, 2020; OMIM 2021 [Web]; Weil et al, 1995; Lu et al, 2018)

Table 1. Characterization of *MYO7A* (OMIM 2021 [Web]; HGNC 2021 [Web]; NCBI 2021 [Web]; French et al, 2020; Adato et al, 1997)

Symbol	Name	Gene ID	OMIM Ref	Also Known As	Chromosomal Location	Transcripts	Exons
MYO7A	Myosin VIIA	4647	#276900	DFNB2; MYU7A; NSRD2; USH1B; DFNA11; MYOVIIA	11q13.5	14	49

Figure 1. The MYO7A Gene Network. (Lu et al, 2018)

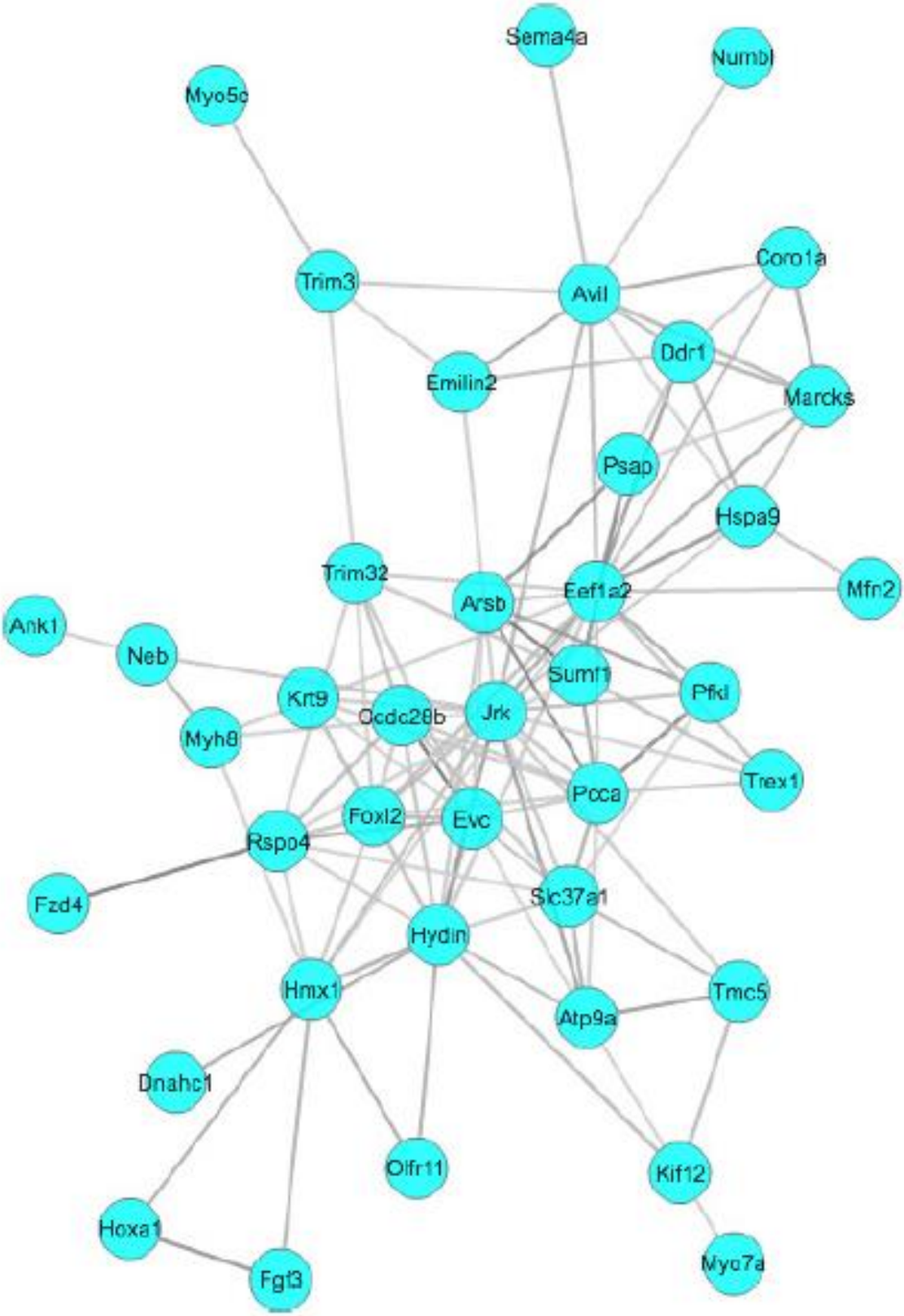

Genes associated with USH, including *MYO7A*, have significant mutational heterogeneity. Pathogenic variants of different natures have been identified, in which the pertinent protein is altered by different molecular pathways. Based on a 2020 analysis of mutations in the USH database from the Leiden Open Variation Database, Fuster-Garcia and colleagues found the most common *MYO7A* pathogenic variants were nonsense, frame shift, and missense (**Figure 2**). (Fuster-Garcia et al, 2021)

Figure 2. Mutation Count in *MYO7A*. (Fuster-Garcia et al, 2021)

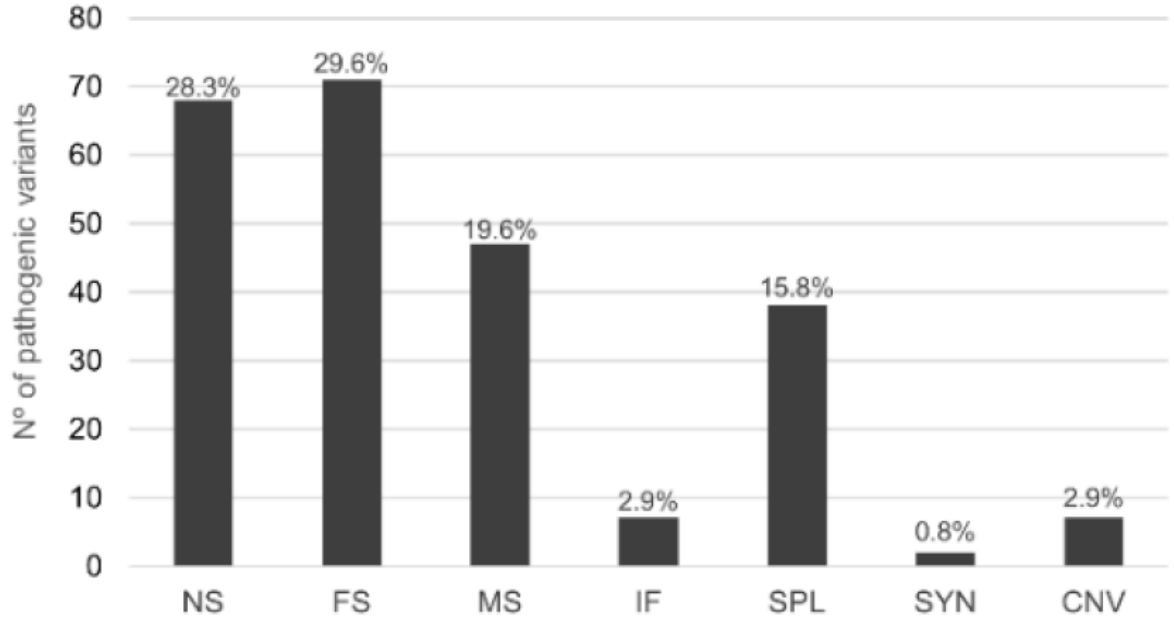

CNV, copy number variant; FS, frameshift variant; IF, in-frame indel variant; MS, missense variant; NS, nonsense variant; SPL, splicing variant; SYN, synonymous.

Pathology

Myosin VIIA Structure

The *MYO7A* gene encodes the myosin VIIA protein, which is included in the unconventional myosin family. Myosins are actin-based motor proteins with adenosine triphosphatase activity that play important roles in diverse cell functions, including cytokinesis; unconventional myosins serve in intracellular molecular transport. The myosin VIIA protein has a motor head domain that interacts with actin; a neck domain with 5 isoleucine-glutamine

(IQ) motifs that bind calmodulin; and a tail domain that includes 2 large tandem repeats of myosin tail homology 4 (MyTH4) and 4.1 ezrin, readixin, moesin (FERM) domains separated by a src homology-3 (SH3) motif. Functions of the myosin VIIA protein head, neck, and tail domains are summarized in **Table 2**. Between the neck and tail domains is a highly charged region, the composition of which remains under debate. Some research indicates the region forms a stable, single α-helix (SAH) domain, which is considered to work as flexible lever arm, whereas other research suggests part of the domain forms a coil, which assists in dimer formation. (Fuster-Garcia et al, 2021; Galbis-Martínez et al, 2021; Kuppa et al, 2021; Li et al, 2017; UniProt 2021 [Web]; Sakai et al, 2015; Sato et al, 2017; Weil et al, 1996)

Table 2. Selected Myosin VIIA Protein Domain Functions. (Kuppa et al, 2021)

Domain	**Function**
Motor head domain	Enables movement of myosin VIIA protein on actin filaments; interacts with ATP and that translates into production of mechanical energy
Neck IQ motifs	Regulate the function of motors in a calcium-regulated manner and acts as the lever of myosin arms
Tail MyTH4 and FERM domains	An N-terminal proline-rich region precedes both MyTH4 and the FERM domains. F1, F2, and F3 lobes are present in each FERM domain; these lobes are known to interact with various integral membrane proteins and connect the cytoskeleton to the plasma membrane of the cell
Tail SH3 motif	Helps in recruiting Arp2/3 complexes, which regulate the actin cytoskeleton; C-terminal proline-rich regions of myosin VIIA can interact with the SH3 domain

A 2008 investigation, in USH1B patients showed that most missense mutations in MYO7A resulted in severe deficiencies in the protein's actin-activated ATPase activities. A subsequent 2021 analysis utilizing global computational mutagenesis to evaluate the impact of missense *MYO7A* mutations on myosin VIIA structure and stability found that the motor domain and MyTH4 domains were the most susceptible to mutations resulting in the USH1B phenotype. (Watanabe et al, 2008; Kuppa et al, 2021)

There are multiple isoforms of the myosin VIIA protein, with 2 isoforms expressed in the human retina (isoform 1, 2215 aa; isoform 2, 2175 aa). The relative isoform expression differs between mouse and human retinas. Whereas isoform 2 is the major isoform in the human retina, it is notable that isoform 1 is not expressed in mouse retinal pigment epithelial (RPE) cells, which has led to speculation regarding the function of isoform 1 in the human retina. (Li et al, 2020; UniProt 2021 [Web]; Weil et al, 1996)

Myosin VIIA Function

Myosin VIIa is expressed in the inner ear, retina, testis, lung, and kidney. In the inner ear, myosin VIIa expression is restricted to the inner and outer hair cells and is essential for the development of the hair bundle of the cochlea and vestibular system, and for mechanoelectrical transduction in the hair cells. There is some debate over the localization of MYO7A expression in the eye across species. In the mouse, the protein is found in the RPE, where it localizes in the apical region, and in the rod and cone photoreceptors, where it is localized to the connecting cilium and periciliary region (**Figure 3**). Myosin VIIA also has been reported to be present in the calyceal processes of monkey and frog photoreceptors. Calyceal processes have not been observed in the mouse retina. (Hasson et al, 1995; Liu et al, 1997; Self et al, 1998; Kros et al, 2002; Boëda et al, 2002; Williams 2008; Sahly et al, 2012; Lopes et al, 2015)

Figure 3. Myosin VIIA function in the RPE Cell and Localization in Photoreceptor Cells. (Williams et al, 2011)

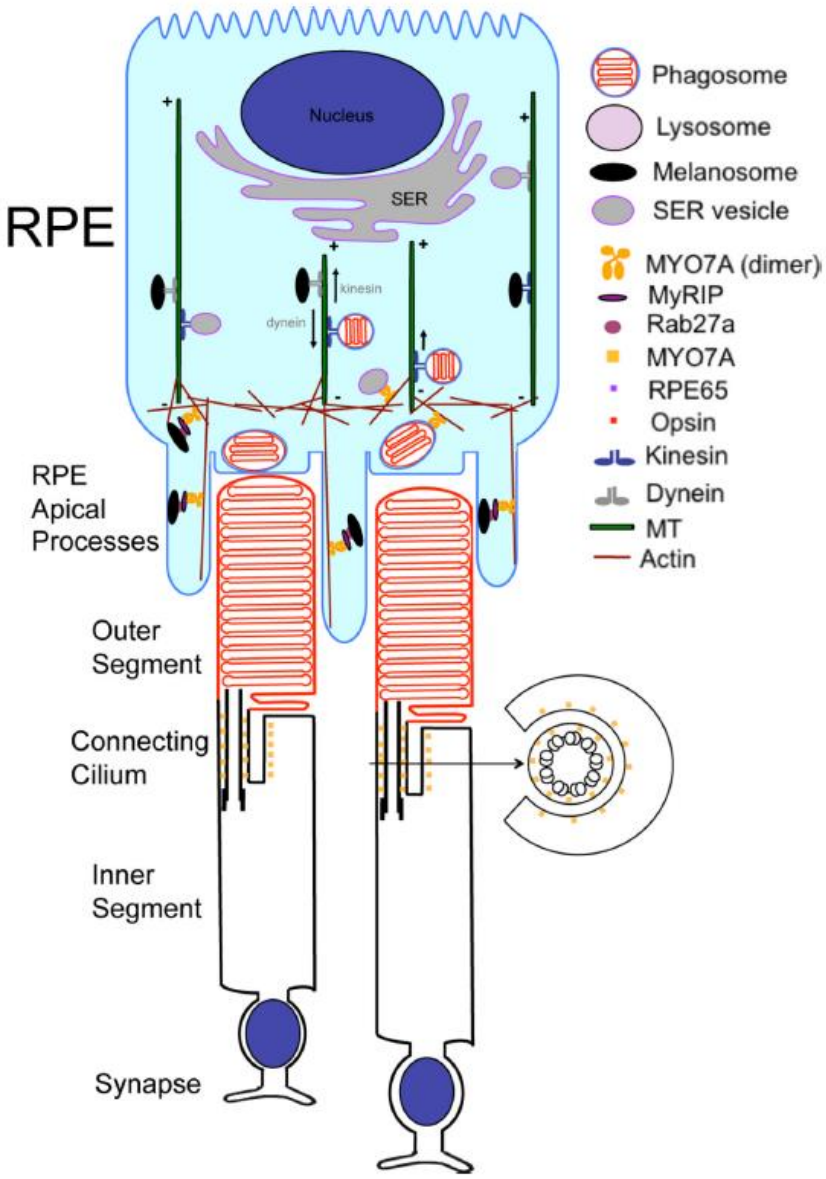

Among its multiple functions, myosin VIIA has been shown to be involved in melanosome and phagosome transport in the RPE and in opsin transport through the cilium in mouse photoreceptors. In the mouse RPE, evidence indicates that myosin VIIA and Rab–interacting protein (MYRIP) links Ras-related protein Rab-27A (RAB27A) on melanosomes to myosin VIIA. Without myosin VIIA (or either linker protein), the melanosomes are unable to move along actin filaments and are absent from the apical RPE. Myosin VIIA associates with RPE phagosomes and contributes to their motility,

with lack of the protein resulting in slowed degradation of these organelles. In the photoreceptors of *shaker1* mice (a model of USH1B), detailed analysis by immunoelectron microscopy has shown that the ciliary plasma membrane has an abnormal accumulation of rhodopsin, suggesting a role for myosin VIIA in facilitating opsin delivery to the disk membranes of the photoreceptor outer segment. Myosin VIIA also has been implicated in the light-dependent translocation of the retinoid isomerase, RPE65, in the RPE. (Liu et al, 1999; Gibbs et al, 2003; Klomp et al, 2007; Lopes et al, 2007; Lopes et al, 2011; Williams et al, 2011; Lopes et al, 2015)

Disease Models

The *MYO7A* gene is conserved in chimpanzee, Rhesus monkey, dog, cow, mouse, rat, chicken, zebrafish, fruit fly, and frog. (NCBI 2021 [Web])

Mouse

The mouse model is the most commonly utilized in USH, including USH1B (**Table 3**). Due to the high conservation between the genetic pathways that regulate auditory perception in mice and humans, all currently available USH mutant mice well mimic the impairment of human hearing. Each of these reproduces the characteristic early-onset hearing loss and vestibular defects as found in individuals with USH1. Although localization and function of myosin VIIA in human RPE cells is comparable to that in mouse RPE cells, none of the mouse models for USH1B show retinal degeneration. In general, USH mouse models poorly recapitulate the visual deficiencies manifested in humans when the orthologous genes are disrupted, potentially because the calyceal processes and periciliary membranes are absent or underdeveloped in mouse photoreceptors compared with human photoreceptors (Fuster-Garcia et al, 2021; Sahly et al, 2012; Gibbs et al, 2010)

Table 3. Summary of Described Mouse Models of USH1B (*MYO7A*). Some models were characterized without describing retina outcomes, the absence of these data is noted as not available (N/A) under retinal degeneration. (Gibson et a, 1995; Mburu et al, 1997; Ernest et al, 2000; Rhodes et al, 2004; Schwander et al, 2007; Schwander et al, 2009; Miller

et al, 2012; Wasfy et al, 2014; Calabro et al, 2019; Fuster-Garcia et al, 2021).

Model	Hearing Loss	Vestibular Dysfunction	Retinal Degeneration
Myo7a$^{sh1/sh1}$ (shaker1)	Yes	Yes	No
Myo7a$^{hdb/hdb}$ (headbanger)	Yes	Yes	N/A
Myo7a$^{pk/pk}$ (polka)	Yes	Yes	No
Myo7a$^{I487N/I487N}$ (ewaso)	Yes	Yes	N/A
Myo7a$^{F947I/F947I}$ (dumbo)	Yes	No	N/A
Myo7a$^{-/-}$	Yes	Yes	No

Shaker1 Mouse

The *shaker1* mouse, which is homozygous for an early nonsense mutation in *MYO7A*, is the most commonly used USH1B model. Although there is no overt retinal degeneration observed, *shaker1* mice show subtle retinal phenotypes, including:

- Mislocalization of melanosomes that do not enter into the RPE microvilli (Liu et al, 1998)
- Slower transport of rhodopsin that accumulates at the photoreceptor connecting cilium and slower distal migration of photoreceptor outer segments (Liu et al, 1999)
- Abnormal phagocytosis of photoreceptor outer segment disks by the RPE (inhibited transport of ingested disks out of the apical region) (Gibbs et al, 2003)
- A delay in photoreceptor ability to recover from light desensitization and progressive reduction of b-wave electroretinogram (ERG) amplitude and light sensitivity (Colella et al, 2013)
- Moderate light–induced oxidative damage and rod degeneration with delayed rod transducin translocation (Peng et al, 2011)

However, unlike individuals with USH1B, who manifest severe ERG decline and photoreceptor degeneration, *shaker1* mice do not present with either

photoreceptor cell loss up to 24 months of age or significant ERG reduction, which is also true of other USH1B models. (Colella et al, 2013)

Myo7a-/-

Researchers generated a new transgenic MYO7A KO mouse (*Myo7a*$^{-/-}$) that was confirmed to be null for MYO7A in both the eye and inner ear (Calaboro et al, 2019). Analyzing the homozygous knockout versus the heterozygous knockout compared to the wildtype mice, haploinsufficiency was observed in the heterozygotes with regard to hearing defects (loss of inner-hair cells (cochlear and vestibular hair cells). Similar to the Shaker mouse the homozygous knockout mice have normal retinal structure and function. The *Myo7a*$^{-/-}$ mice still serve as a suitable model for testing dual AAV recombination efficiency.

Zebrafish

Unlike mouse models, the *myo7a*$^{m/m}$ (or *myo7aa*$^{-/-}$; mariner) zebrafish model of USH1B exhibits hearing loss, vestibular dysfunction, and retinal degeneration. The zebrafish (*Danio rerio*) possesses 2 mechanosensory organs believed to be homologous to each other: the inner ear, which is responsible for the senses of audition and equilibrium, and the lateral line organ, which is involved in the detection of water movements. Eight zebrafish circler or auditory/vestibular mutants appear to have defects specific to sensory hair cell function. The phenotype of the circler mutant, mariner, is due to mutations in *MYO7A*. Analysis of the fine structure of hair bundles in mariner mutants suggested that a missense mutation within the C-terminal FERM domain of the tail of myosin VIIA has the potential to dissociate the protein's 2 functions in hair bundle integrity and apical endocytosis. Mariner sensory hair cells display morphological and functional defects that are similar to those present in *shaker1* mice. In the retina, mariner zebrafish exhibit elevated cell death, mislocalization of rods and blue cone opsins and reduced expression of rod-specific markers in the outer nuclear layer. Electroretinogram recordings show a significant decrease in both a- and b-wave amplitudes (**Figure 4**). (Fuster-Garcia et al, 2021; Ernest et at, 2000; Wasfy et al, 2014)

Figure 4. Mariner Zebrafish Mutants Show Reduced Visual Function. (Wasfy et al, 2014)

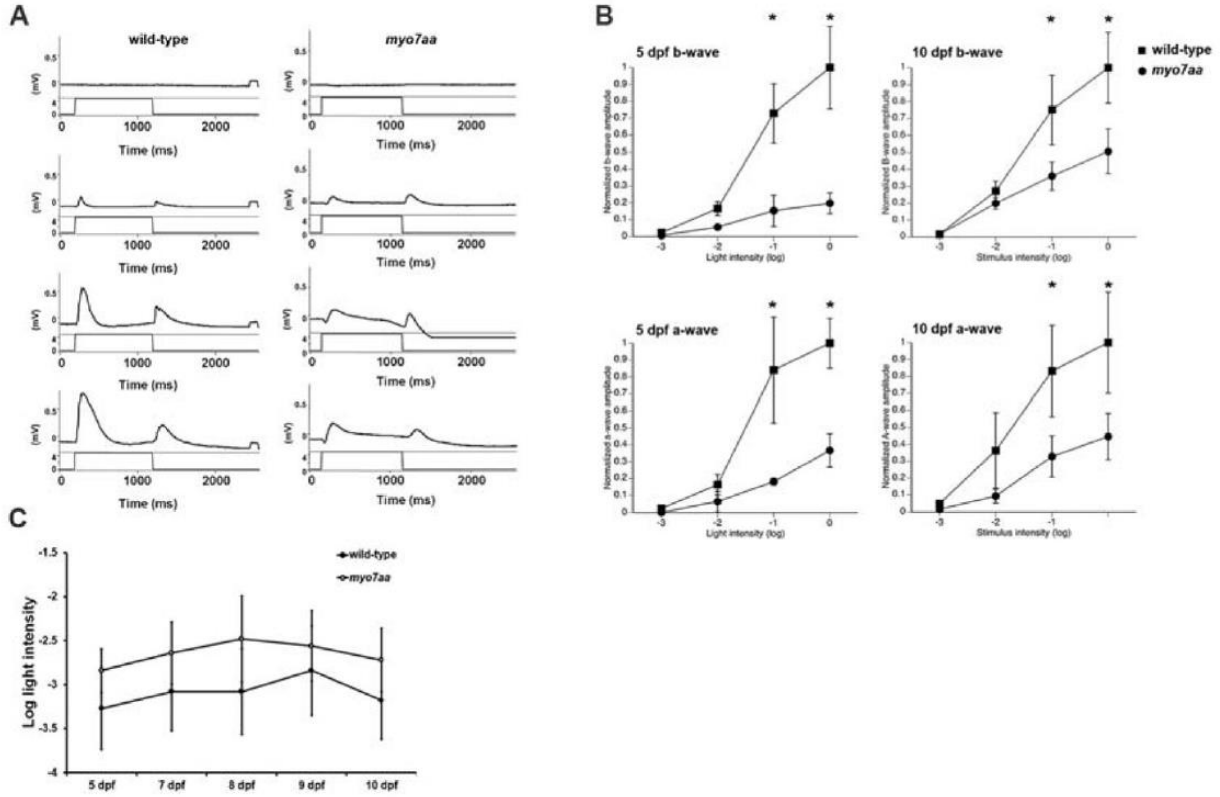

(**A**) Representative ERG recordings from wild-type (left) and *myo7aa*$^{-/-}$ mutants (right) under constant background illumination following 1000-millisecond light stimuli at increasing light intensities over a range of 4 log units. (**B**) Normalized ERG b-wave (top) and a-wave amplitudes (bottom) to increasing light stimuli. Both the b-wave and a-wave amplitudes were reduced in the *myo7aa*$^{-/-}$ mutants, although thresholds were unchanged (*P<0.05). (**C**) Dark adapted optokinetic response (OKR) in 5–10 dpf wild-type and *myo7aa*$^{-/-}$ larvae (P>0.05). During a 30-second trial, the light intensity required to generate a positive OKR response was determined. The unattenuated light stimulus (log I = 0) was 9.74×10^{-2} μW/cm2. In all cases, error bars represent standard error of the mean.

Potential Future Models

Derks et al recently reported a natural knockout of the *MYO7A* gene in pigs. The variant identified (NM_001099928.1:c.541C>T) results in a stop codon at position p.Gln181* in the protein, resulting in impaired and truncated myosin VIIA. Piglets homozygous for the stop-gained *MYO7A*

variant suffer from balance difficulties that usually result in death within the first 10 days after birth during the weaning period. Furthermore, the study showed indications that the variant might lead to deafness in (older) heterozygous carrier animals. (Derks et al, 2021)

Research is ongoing at Oregon Health & Science University to create a non-human primate model of USH1B.

Epidemiology

The reported prevalence range for USH is 1.5-6.2/100,000 depending on the study and population, but this range may be an underestimate. A US study by Kimberling and colleagues among 2 populations comprising 133 high school students who were deaf or hard of hearing found 11.3% carried an USH-associated mutation. Utilizing a conservative estimate of the frequency of childhood deafness of ~1/1000, these authors estimated USH prevalence in the US population of 1 in 6000 (16.7/100,000). (Millán et al, 2011; Stephenson et al, 2019 [Congress presentation]; Kimberling et al, 2010)

The epidemiology of USH1B specifically is not well-characterized. However, a 2019 systematic review and meta-analysis of data from 11 next-generation sequencing studies in 684 patients with USH found 21% had mutations in *MYO7A*, which could provide a basis to extrapolate global USH1B prevalence (range: 0.3-3.5/100,000 based on the estimates above). (Jouret et al, 2019)

Clinical Manifestations

Usher syndrome type 1 is characterized by congenital, bilateral, severe-to-profound sensorineural hearing loss, vestibular dysfunction, and RP. Unless fitted with a cochlear implant, individuals do not typically develop speech. Although the timing and extent of vestibular dysfunction is not fully understood, children with USH1 typically walk later than usual, at approximately age 18 months to 2 years. RP develops in adolescence, resulting in progressively constricted visual fields and impaired visual acuity. (Koenekoop et al, 2020)

In a 2009 study, Jacobson and colleagues assessed the retinal microstructure and visual sensitivity of 17 individuals (age range, 4-61 y) with USH1B utilizing optical coherence tomography (OCT) and automated perimetry. They found a wide range in degree of laminar architecture abnormality. The first detectable retinal abnormality was increased outer limiting membrane prominence. Visual loss was related to a decline in outer nuclear layer thickness (**Figure 5**), which was accompanied by increased outer plexiform layer thickness and normal or increased inner nuclear layer. (Jacobson et al, 2009)

Figure 5. Retinal Thickness Topography in USH1B. (Jacobson et al, 2009)

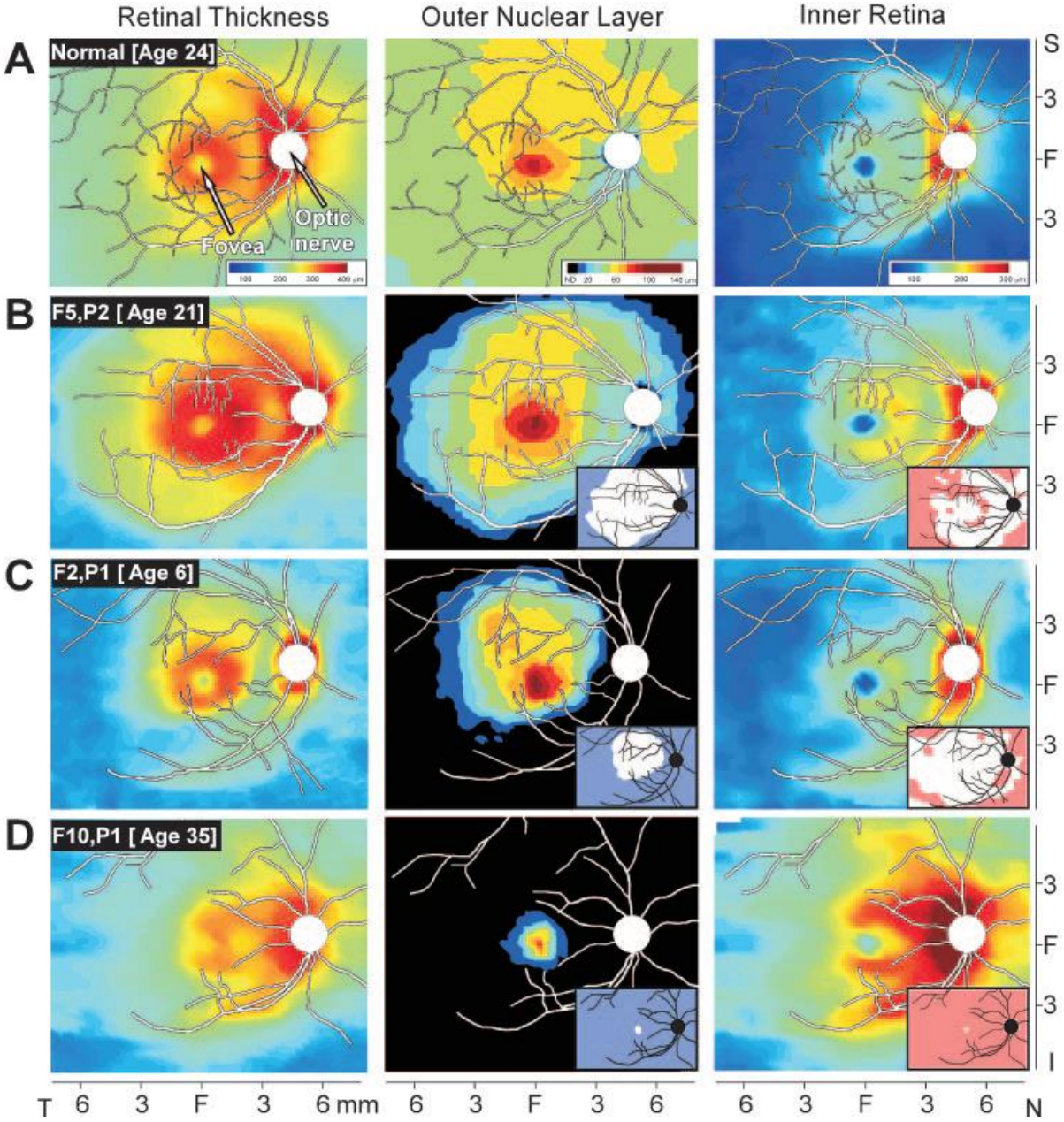

Topographical maps of total retinal (*left*), ONL (*middle*), and inner retinal (*right*) thicknesses in a normal 24-year-old individual (**A**) and 3 people with *MYO7A*-USH1B of different ages and disease stages (**B**–**D**). Traces of major blood vessels and location of optic nerve head are overlaid on each map (depicted as right eyes). Pseudocolor scales are shown beneath the normal maps. *Insets:* thickness difference maps showing regions that were abnormally thin (*blue*), within normal limits (*white*, defined as mean ± 2 standard deviation), or thick (*pink*), compared with normal. Optic nerve

outlines were schematized in both the topographic and thickness difference maps. T, temporal; N, nasal; S, superior; I, inferior, F, fovea.

In their 2008 paper, Jacobson and colleagues found evidence from 2 individuals in 2 different families that the structural abnormalities (measured at 4.1 mm in the superior retina) begin in the photoreceptors before the RPE. In one subject, the below-normal photoreceptor signal at age 8 had completely disappeared at age 15, while the RPE signal remained stable within normal limits. Similarly, a second subject at age 17 had lower than normal photoreceptor signal that was completely absent at age 25, while the RPE signal was stable and normal at both ages.

In a 2020 study, Subirà and colleagues described retinal alterations detected by swept-source OCT in children with USH1B (n=16, age range, 4-17 y [mean, 11.3 y]). They found that external layer damage (ELM loss, EZ disruption, OS loss) in the macula was the most common retinal abnormality. Retinal pigment epithelial damage was found in the phagosome zone (30 eyes; 93.8%) and melanosome zone (29 eyes; 90.6%) but not in the mitochondria zone (**Table 4**). Cystoid macular edema was correlated with alterations in the photoreceptors, and disruption or absence of the myoid and ellipsoid zones were correlated with decreased visual acuity. (Subirà et al, 2020)

Table 4. Qualitative Retinal Alterations in the Macular Area in Individuals with USH1B
(Eyes, n=32). (Subirà et al, 2020)

Retinal Observation	Frequency (n, %)
Altered	
Internal lining membrane	9 (28.1)
Present	
Epiretinal membrane	0
Retinal micropseudocysts	15 (46.9)
Cystoid macular edema	8 (25)
Absent	
External limiting membrane	27 (84.4)
Myoid zone	27 (84.4)
Ellipsoid zone	28 (87.5)
Cone outer segments	29 (90.6)
Phagosome zone	30 (93.8)
Melanosome zone	29 (90.6)
Mitochondria zone	0

Also in 2020, Small and colleagues used confocal and non-confocal adaptive optics scanning laser ophthalmoscopy to observe the cone photoreceptor mosaic in 4 individuals with USH1B (age range, 8-37 y; mean 19 y). Imaging showed cone mosaics in 3 individuals; the oldest person had severe photoreceptor degeneration and cystoid macular edema. All individuals who underwent imaging had regions of interest (selected at locations where measurable cones were visible) with cone spacing Z-scores >2, but the fraction of these regions with normal cone spacing was large (>84%). Fibroblasts (skin cells) from USH1B patients were converted into induced pluripotent stem cells (iPSCs) then differentiated in RPE cells. Western blot data showed no evidence of myosin VIIA protein production in these cells. (Small et al, 2020 [Congress presentation])

Natural History

Jacobson and colleagues reported on retinal disease at a single time point in 33 individuals (25 families) from the United States aged 2-62 years with USH1B and *MYO7A* mutations. In this cohort, rod-mediated vision could be lost to different degrees in the first decades of life, whereas cone vision followed a more predictable and slower decline. Central vision ranged from normal to reduced in the first 4 decades of life but was severely abnormal thereafter. Photoreceptor layer thickness in a wide region of central retina could differ dramatically between individuals of comparable ages, and there were examples of severe losses in childhood but relative preservation in the third decade of life (**Figure 6**). Patients with stop mutations within the coding region of the MYO7A motor domain tended to have relatively milder rod disease. (Jacobson et al, 2011)

Figure 6. Retinal Structure in USH1B. (Jacobson et al, 2011)

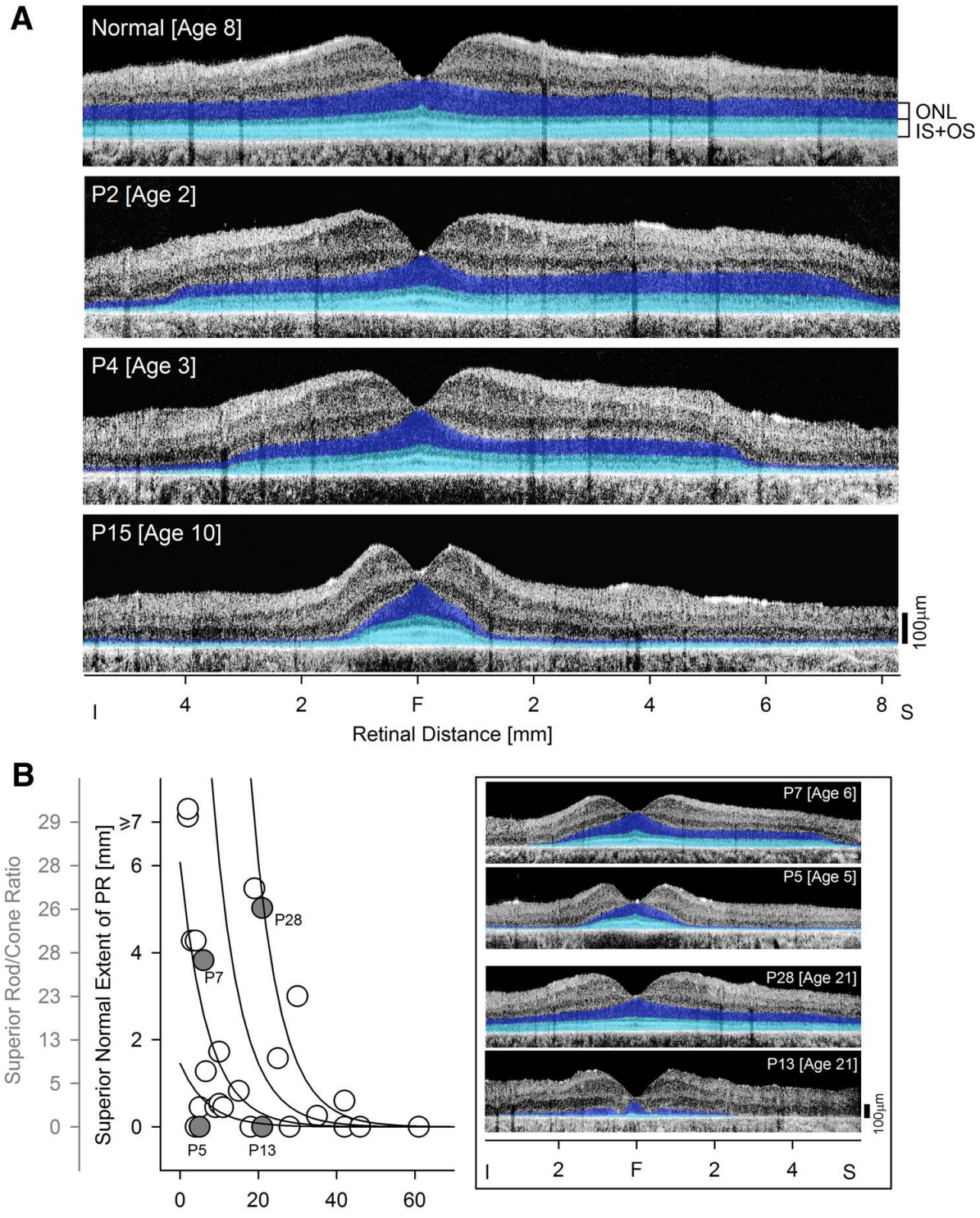

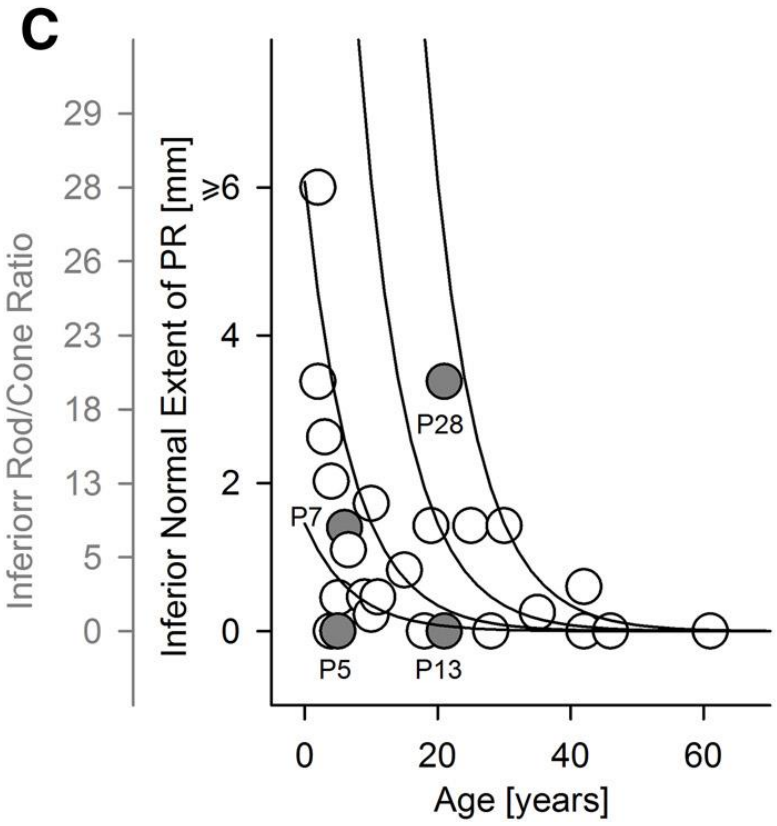
C
Inferiorr Rod/Cone Ratio
29
28
26
23
18
13
5
0
Inferior Normal Extent of PR [mm]
≥6
4
2
0
P28
P7
P5
P13
0
20
40
60
Age [years]

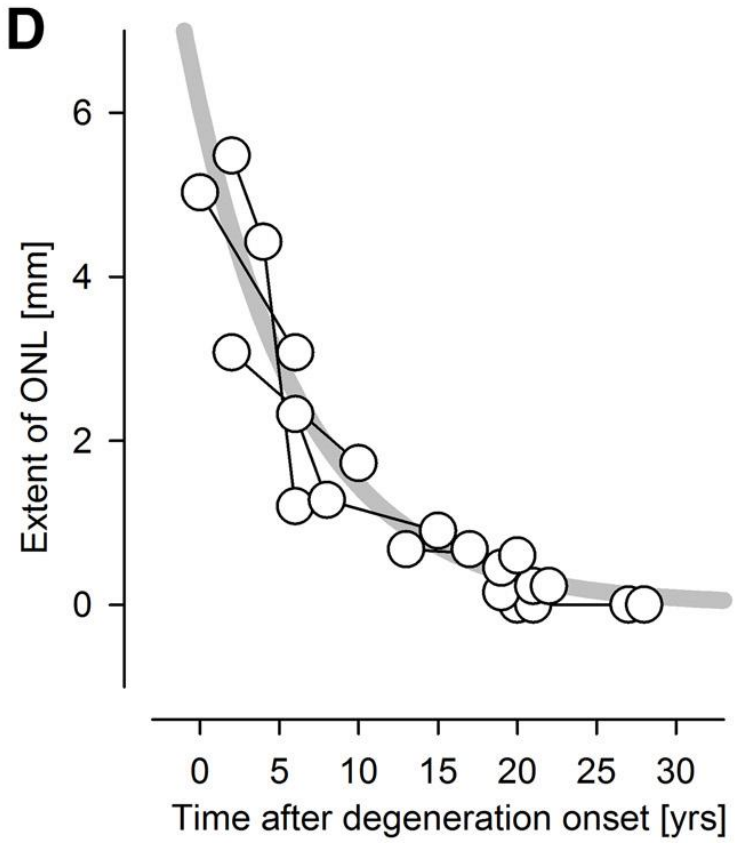
D
Extent of ONL [mm]
6
4
2
0
0
5
10
15
20
25
30
Time after degeneration onset [yrs]

(**A**) SD-OCT scans along the vertical meridian through the fovea in a representative normal subject and USH1B patients P2, P4, and P15. Photoreceptor (PR) layers are colorized for visibility: ONL (*dark blue*) and inner and outer segments (*light blue*). (**B**) *Left*: superior extent of normal PR layer thickness along the vertical meridian in all USH1B patients with SDOCT results. *Lines*: invariant exponentials delayed along the time axis by 1-decade intervals. *Gray symbols*: the patients shown to the *right*. *Gray axis* (*left*): the rod/cone ratio in normal human eyes as a function of eccentricity. *Right*: SD-OCT scans from pairs of USH1B patients with similar ages but dissimilar extents of normal PR structure demonstrating interindividual variation of disease severity. (**C**) Inferior extent of normal PR layer thickness along the vertical meridian in all USH1B patients with SD-OCT results. *Lines*, *gray axes*, and *gray symbols* are as described in (**B**). (**D**) Longitudinal measurements of ONL thickness along the vertical meridian superior to the fovea using TD-OCT in a subset of eight USH1B patients. Data from each patient are shifted along the time axis to partially overlap with one another. *Gray line*: exponential fit to the resulting data set. The same exponential is redrawn in (**B**) and (**C**).

A later study from the same group of researchers studied ellipsoid zone (EZ) changes on OCT as a method of assessing disease natural history in 16 US individuals with USH1B and MYO7A mutations (age range, 2-42 y). Serial measurements were available for 8 individuals. They found EZ extent constricted at a rate of 0.51°/year, with slower rates at smaller initial eccentricities (**Figure 7**). A well-defined EZ line could be associated with normal or abnormal outer nuclear layer (ONL) and/or outer segment thickness; detectable ONL extended well beyond EZ edge. Based on their findings, they recommended combining the EZ line with other structural and functional parameters to assess disease natural history. (Sumaroka et al, 2016)

Figure 7. EZ Extent and Annual Rate of Constriction in Different Retinal Regions of USH1B. (Sumaroka et al, 2016)

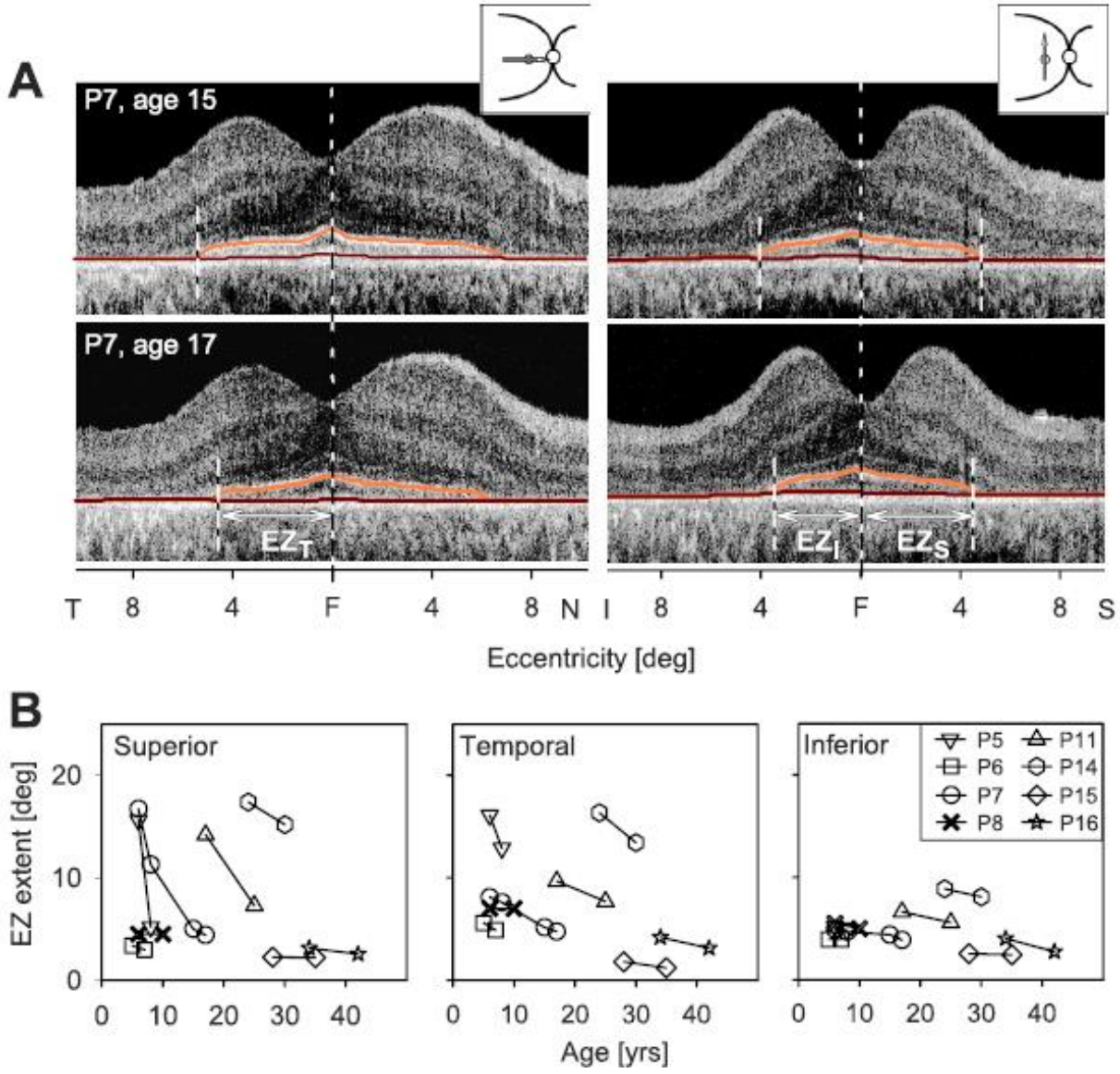

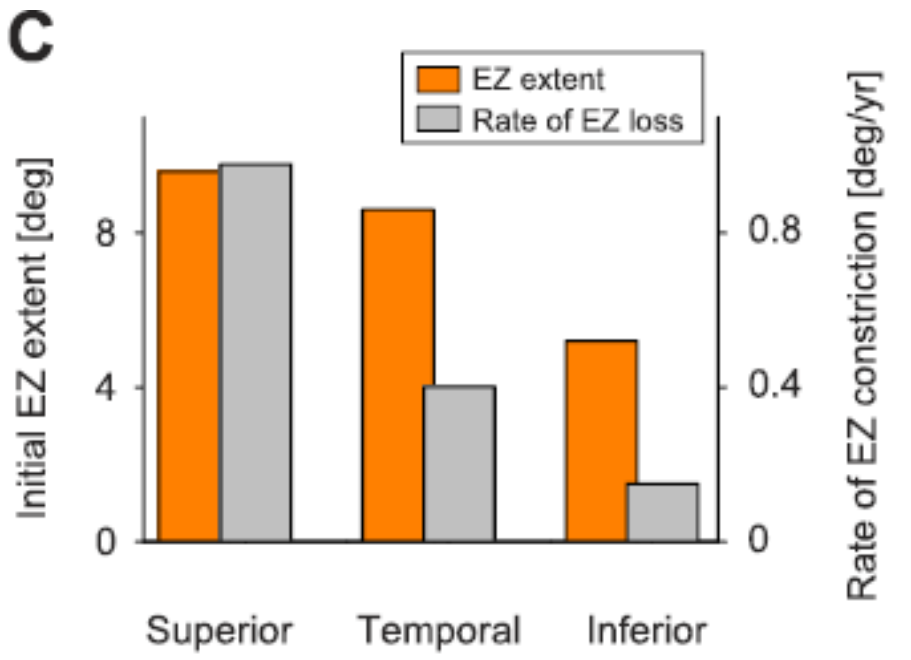
C
EZ extent
Rate of EZ loss
Initial EZ extent [deg]
Rate of EZ constriction [deg/yr]
8
4
0
0.8
0.4
0
Superior
Temporal
Inferior

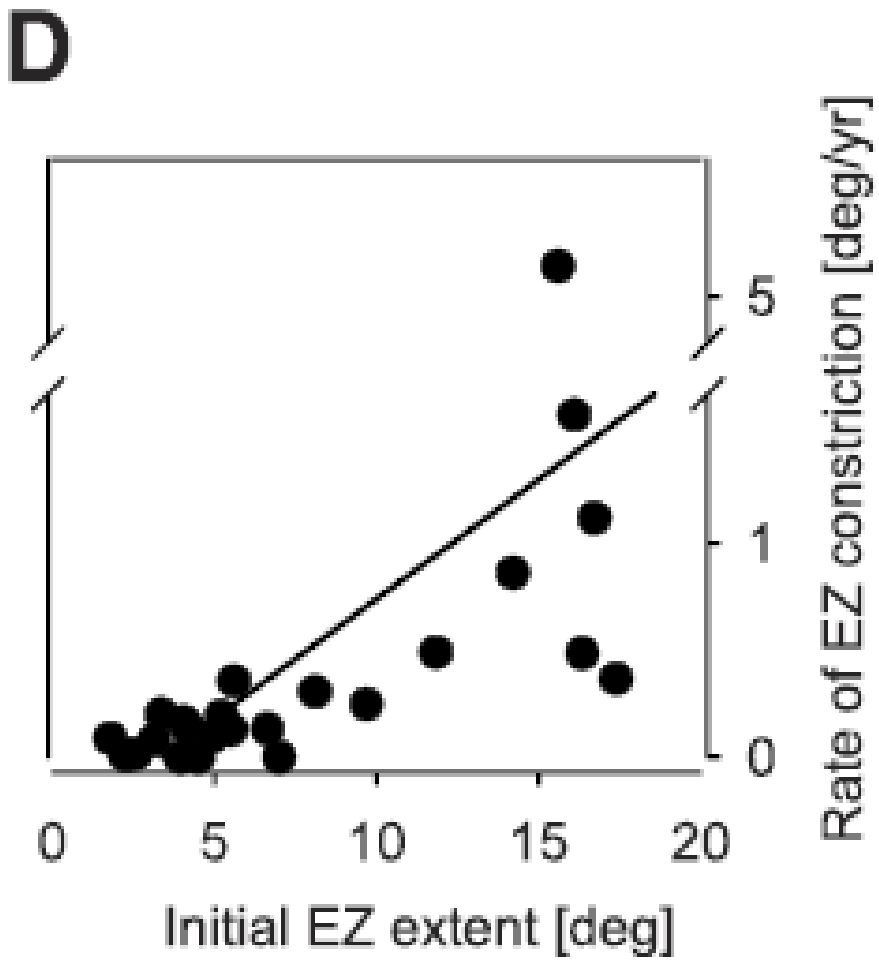
D
Rate of EZ constriction [deg/yr]
5
1
0
0
5
10
15
20
Initial EZ extent [deg]

(**A**) OCT scans along horizontal (*left*) and vertical (*right*) meridians through the fovea for P7 at ages 15 (*top*) and 17 (*bottom*). The EZ line is highlighted in *orange* and the RPE inner boundary in *dark red*. Ellipsoid zone extent is measured along temporal (EZ_T), superior (EZ_S), and inferior (EZI) meridians. *Icons*: locations of cross-sectional scans. (**B**) Ellipsoid zone extent versus age for eight USH1B patients (ages 5–34 at first visit) along the 3 meridians; longitudinal data are connected by lines. (**C**) Average of initial EZ extents (*orange bars, left axis*) and the average rate of EZ constriction (*gray bars, right*) for the 3 retinal regions. (**D**) Individual rates of EZ constriction as a function of initial EZ extent. *Black line is the regression line*.

Lenassi and colleagues investigated the natural history of retinal disease in 28 (26 families) individuals from the United Kingdom with 2 likely disease-causing variants in *MYO7A* and USH1 symptoms (age range, 3-65 y; median, 32 y). Longitudinal visual acuity and fundus autofluorescence data (FAF) were followed over a 3-year period for a subset of individuals. They found that visual acuity was significantly correlated with age (P<0.0001; r=0.71). Visual acuity ≤0.22 logMAR was maintained in 50% of individuals until age 33.9 years, and legal blindness based on loss of acuity or field was reached at a median age 40.6 years. Although several individuals had a milder phenotype, there were no obvious genotype-phenotype correlation. (Lenassi et al, 2014)

A retrospective study compared the clinical presentation and disease course for 43 individuals from Italy with 2 disease-associated mutations in *MYO7A* (USH1 diagnosis; n=10 from 7 families) or *USH2A* (USH2 diagnosis; n=33 from 31 families). Longitudinal analysis was over a median follow-up time of 3.5 years. Individuals with *MYO7A* mutations had a younger age of onset of hearing and visual impairments compared with those carrying mutations in *USH2A*, leading to an earlier diagnosis. Individuals carrying *MYO7A* mutations experienced more rapid declines in visual acuity and visual field (**Table 5**) and reached legal blindness on average 15 years earlier than those carrying *USH2A* mutations. (Testa et al, 2017)

Table 5. Annual Rate of Disease Progression in Individuals With USH1B and USH2A. (Testa et al, 2017)

	USH1B				USH2A				USH1B vs. USH2A			
Feature	Mean	SEM	G. Mean	*P*	Mean	SEM	G. Mean	*P*	Mean	SEM	G. Mean	*P*
Log BCVA	−0.040	0.0038	−3.92	<**0.001**	−0.035	0.0030	−3.44	<**0.001**	−0.005	0.0024	−0.50	**0.025**
Log visual field area	−0.089	0.018	−8.52	<**0.001**	−0.051	0.0106	−4.97	<**0.001**	−0.038	0.0138	−3.73	**0.005**
Log ERG amplitude (photopic)	−0.084	0.029	−8.06	**0.004**	−0.028	0.010	−2.76	<**0.001**	−0.021	0.0155	−2.08	0.172

G. Mean, geometric mean; SEM, standard error of mean. The *p*-values are bold where they are less than or equal to the significance level cut-off of 0.05.

A study by Mohand-Said and colleagues investigated the natural history of retinal disease in 45 individuals (38 families) with USH1B (age range, 9-61 y) followed at the CHNO des Quinze-Vingts in Paris, France. They found visual acuity decreased with advancing age but was preserved until about age 50 years. Visual field loss followed a pattern similar to non-syndromic RP, initially showing scotomas deepening in mid-periphery in the first decade, and progressively coalescing and extending. The residual tubular VF also was progressively reduced over time. Rate of cystoid macular edema was 67% in individuals under age 20 years, 29% for those aged 21 and 40 years, and 17% for those aged >40 years. This group conducted a second natural history study at the same center among individuals with USH1B (n=15; age at first visit, 34 y) and USH2A (n=28; age at first visit, 42 y). With 2 years of follow-up data, they found individuals with USH1B had a younger age of onset of visual impairment; however, vision loss over the 2 years did not differ between groups. (Mohand-Said et al, 2017 [Congress presentation]; Mohand-Said, 2018 [Congress presentation])

The UshTher consortium is conducting a multicenter, longitudinal (2-year) natural history study among individuals aged 8 years and older with USH1B (N=44; age range, 9-72 years) in Europe. Cross-sectional analysis showed a decline with age of best-corrected visual acuity at a mean annual rate of 0.015 logMAR/year equivalent to about 1 EDTRS letter/year (*P*<0.001); of visual field at 3.8%/year (*P*<0.001); and of macular sensitivity at -3.8%/year (*P*=0.003). There was a less pronounced (*P*=0.099) decline of the EZ band width (-1.7%/year). (Testa et al, 2020 [Congress presentation])

Characterized Clinical Cohorts

Europe + Morocco

Screening from mutations in *MYO7A* among 40 individuals with USH1 from Italy, Spain, Turkey, the Czech Republic, and Morocco revealed 19 likely pathogenic mutations, with 13 not previously prescribed (**Table 6**). Mutations were detected in 14 of the 40 families studied, accounting for 35%. No mutation was detected in those patients where a diagnosis of USH1 could not be confirmed. Excluding these individuals, *MYO7A* was responsible for 45% of USH1 in the cohort. (Jaijo et al, 2007)

Table 6. Genotypes of Individuals with USH1B From Different Countries. (Jaijo et al, 2007)

Genotype/patient	Mutation 1	Mutation 2	Origin
Homozygous			
RP-1264	c.5835_5838delCTTT	c.5835_5838delCTTT	Italy
RP-1283*	p.P132L	p.P132L	Spain
RP-1301	c.2283-1G>T	c.2283-1G>T	Morocco
RP-1340*	p.I219_H220del	p.I219_H220del	Spain
RP-1356	p.I1045T/p.L1836P	p.I1045T/p.L1836P	Italy
RP-1462*	p.R241G	p.R241G	Italy
Compound heterozygous			
RP-1252*	c.3764delA	p.R1861X	Spain
RP-1266*	p.A26E	p.L366P	Italy
RP-1268	p.N330QfsX5	p.R1240Q	Italy
RP-1269	p.R241G	c.6025delG	Italy
RP-1271	p.R241G	p.G1218R	Italy
RP-1436	p.C628X	c.4297delC	Spain
Heterozygous			
RP-1293	p.A1492V	ND	Spain
RP-1426	p.A2204P	ND	Spain

ND, not determined.
*Patients in whom segregation analysis was performed.

France

An analysis of 53 individuals (from 42 families) with USH1 with biallelic *MYO7A* mutations revealed 50 different genetic variations, 4 of them novel. Functional visual characteristics of these individuals, most of whom showed a rod-cone dystrophy phenotype, followed the typical linear decline pattern, but structural changes based on spectral domain OCT, short wavelength

autofluorescence, and near-infrared autofluorescence measurements did not correlate with age. There were no substantial genotype-phenotype correlations. (Khateb et al, 2020)

Macano, Venezuela

The population of the Macano peninsula of Margarita Island in Venezuela has perhaps the greatest incidence of USH1B known in Latin America (76.9/100,000 population). The initial clinical, genetic, and socioeconomic assessment of this population identified 24 sibships from 4 villages (N=329). Thirty-six participants were found to have congenital abnormalities, 15 with bilateral sensorineural hearing loss, RP, and vestibular areflexia. The average age of onset of eye symptoms was 7 years. These 15 patients belonged to 6 families in which the disease distributed horizontally, with frequent generation skips; parents were phenotypically normal; and there were nine first cousin marriages. One family had 4 deaf-blind children out of 9. Genome-wide linkage analysis identified a locus on chromosome 11q, band 13.5, with a maximum LOD score (Z_{MAX}) of 6.76 at D11s4186; Θ = 0.00. All markers with significantly positive logarithm of odds of linkage (LOD) scores (**Table 7**) flanked a 0.5-1.0 centi Morgan interval containing the gene *MYO7A*. (Keough et al, 2004)

Table 7. Polymorphic Markers and Maximum LOD scores (Θ = 0.00) on Chromosome 11. (Keough et al, 2004)

Marker	Maximum LOD Score	Chromosome	Arm	Region/Subregion
D11s527	6.55	11	q	13.5
D11s4186	6.76	11	q	13.5
D11s911	6.08	11	q	13.5
D11s2011	5.45	11	q	13.5

A subsequent analysis of individuals from this cohort found a novel mutation named c.6079_6081del was detected on exon 45 of the MYO7A gene, causing the loss of a single histidine amino acid at codon 2027 (p.H2027del) located within the second FERM domain of the human protein

myosin VIIA. Three patients with clinical diagnosis of USH1B were detected positive in homozygosis for the c.6079_6081del mutation. Six people from the same affected family were heterozygotes. (Guzmán et al, 2016)

Spain (Jaijo)

Among a cohort of 48 families with 75 individuals diagnosed with USH1 referred from the Federacion de Asociaciones de Distrofias de Retina de Espana (FARPE) and from several Spanish hospitals, 25 different *MYO7A* mutations were identified, including 12 previously unreported (**Table 8**). (Jaijo et al, 2006)

Table 8. MYO7A Mutations Among a Cohort of Individuals with USH1 in Spain. (Jaijo et al, 2006)

Mutation	Exon	Nucleotide Change	Families (n)
Missense			
p.Ser157Asn	5	c.470G>A	1*
p.Gly214Arg	7	c.640G>A	3
p.Arg336His	10	c.1007G>A	1
p.Gln493Pro	13	c.1478A>C	1*
p.Arg1168Pro	27	c.3503G>C	1*
p.Pro1244Arg	29	c.3731C>G	1*
p.Leu1484Phe	34	c.4450C>T	1*
Nonsense			
p.Arg150X	5	c.448C>T	1
p.Ser210X	7	c.629C>G	1*
p.Arg1373X	31	c.4117C>T	1*
p.Tyr1580X	35	c.4740C>A	1*
Deletions			
p.Ser448LeufsX2	12	c.1342_1343delAG	1*
p.Leu485ArgfsX14	13	c.1454delT	1*
Duplication			
p.Leu4AspfsX39	2	c.6_9dupGATT	1*
Putative Splice-Site Mutation			
p.Lys1952Lys	42	c.5856G>A	1*

*Previously unreported.

Spain (Galbis-Martínez)

The population in this study by Galbis-Martínez et al comprised 62 individuals diagnosed with USH and *MYO7A* mutations from 46 families referred from FARPE and from several Spanish hospitals and recruited at the Genetics Department of the Fundacion Jimenez Diaz Hospital in Madrid. Of these individuals, 3 were classified as having atypical USH or USH2, all of whom had less severe hearing loss with later onset, and one

of whom had no loss of visual acuity at age 65 years. Forty-nine distinct pathogenic/likely pathogenic variants were identified in the 46 families. Patients from 22 of these families were homozygous, and 24 were compound heterozygous. Changes included missense, frameshift, nonsense, small and gross deletions, and variants likely affecting splicing, the most frequent being those leading to a truncated protein (57 out of 92 alleles). Five of the alleles identified in *MYO7A* (10%) had not been previously reported. There was no correlation between genotype and phenotype for *MYO7A*: no statistically significant differences were observed for any variable except for onset of hearing loss due to the 3 individuals with atypical USH and USH2 (**Table 9**). (Galbis-Martínez et al, 2021)

Table 9. Analysis of the Correlation Between Age of Onset for Clinical Features of USH and *MYO7A* Mutation Type. Galbis-Martínez et al, 2021)

Variable	**Group**	**n**	**Mean ± SD**	**Median (IQR)**	***P***
Diagnosis (years)	miss-miss miss-trunc trunc-trunc	13 11 23	11.9 ± 5.9 18.8 ± 10.1 15.1 ± 11.2	11.0 (6.0) 13.0 (14.0) 12.0 (7.5)	0.268
Night blindness (years)	miss-miss miss-trunc trunc-trunc	7 8 22	8.6 ± 3.9 12.6 ± 4.8 14.0 ± 11.0	8.0 (4.5) 10.5 (5.0) 11.5 (6.8)	0.298
Visual field construction (years)	miss-miss miss-trunc trunc-trunc	7 9 24	9.9 ± 5.7 17.3 ± 10.6 13.5 ± 8.7	10.0 (9.0) 14.0 (9.0) 12.0 (4.8)	0.333
Visual acuity reduction (years)	miss-miss miss-trunc trunc-trunc	7 9 17	17.4 ± 10.8 21.1 ± 11.6 22.0 ± 14.5	14.0 (13.0) 20.0 (20.0) 18.0 (22.0)	0.738
Hearing loss (months)	miss-miss miss-trunc trunc-trunc	13 12 25	3.0 ± 5.7 17.9 ± 51.2 0.7 ± 3.6	0.0 (3.0) 1.5 (8.0) 0.0 (0.0)	0.008
Unaided walking (months	miss-miss miss-trunc trunc-trunc	3 6 8	27.7 ± 9.7 17.8 ± 1.5 25.4 ± 11.0	30.0 (9.5) 18.5 (2.5) 21.5 (9.0)	0.220

IQR, interquartile range; miss-miss, missense-missense genotype; miss-trunc, missense-truncating genotype; SD, standard deviation, trunc-trunc, truncating-truncating genotype.

Therapeutic Strategies

Currently, there is no treatment available for USH1B. **Table 10** summarizes therapies under investigation for USH1B, including those for RP and USH that could be applicable to USH1B.

Table 10. Therapies in Development with Potential Applicability to USH1B. (Trapani et al, 2019; de Joya et al, 2021; Atsena Pipeline 2021 [Web]; Atsena USH1B 2021 [Web]; UshTher 2021 [Web]; NCT02556736 [Web]; NCT04278131 [Web]; Martel 2020 [Congress presentation]; Hutton 2021 [News]; Eyevensys 2021 [Press release]; Novartis 2020 [Press release]; Dugel 2019 [Congress presentation]; Kuppermann et al, 2020 [Congress presentation]; Weiss et al, 2019; NCT04355689 [Web])

Gene Therapies				
Agent	**Vector**	**Developer**	**Stage**	**NCT#**
SAR421869 (UshStat)	LV	Sanofi; Oxford Biomedica	Phase I/IIA (terminated)	NCT01505062, NCT02065011
NR	Dual AAV	Atsena Therapeutics	Preclinical	N/A
NR	Dual AAV	UshTher	Preclinical	N/A
BS01*	Recombinant AAV	Bionic Site	Phase I/II	NCT04278131
GS030*	AAV2.7m8	GenSight Biologics	Phase I/II	NCT03326336
MCO-010*	AAV2	Nanoscope Therapeutics	Phase II	NCT04919473; NCT04945772
RST-001*	NR	AbbVie (Allergan)	Phase I/II	NCT02556736
EYS611*	Non-viral	Eyevensys	Preclinical	N/A

N/A*	AAV	Novartis (Vedere Bio)	Preclinical	N/A
Cell-Based Therapies				
Agent		**Developer**	**Stage**	**NCT#**
hRPC therapy*		ReNeuron	Phase I/II	NCT02464436
jCell (hRPC) therapy*		jCyte, Inc.	Phase II	NCT04604899; NCT02320812; NCT03073733
Autologous BMSC†		MC Stem Cells	Phase I/II	NCT03011541
Other				
Agent		**Developer**	**Stage**	**NCT#**
NPI-001†		Nacuity Pharmaceuticals Inc.	Phase I/II	NCT04355689

*For RP not specific to USH1B.
†For USH not specific to type 1B.
AAV, adeno-associated virus; hRPC, human retinal progenitor cell; LV, lentivirus; NR, not reported.

Gene Therapies

SAR421869 (UshStat)

SAR421869 is an equine infectious anemia-virus-based (EIAV) lentiviral vector expressing MYO7A. In the *shaker1* mouse model, subretinal delivery of SAR421869 resulted in production of myosin VIIA in the RPE and photoreceptors and protected photoreceptors from acute and chronic intensity light damage. In the Phase I/IIA clinical trial, SAR421869 was delivered via subretinal injections to patients with USH1B. Sanofi terminated development after review of clinical development plans/priorities and not for safety reasons. In June 2020, Sanofi announced it was

returning the rights to Oxford Biomedica. (de Joya et al, 2021; Zallocchi et al, 2014; Adams 2020 [News])

Dual AAV-Based Agents

The large size of *MYO7A* precludes the use of adeno-associated viruses (AAVs) as vectors due to their relatively small packaging capacity. Recent research has involved the use of dual AAV vector systems for genetic therapy of USH1B. (Lopes et al, 2015; French et al, 2020). The technology splits the gene coding sequence in half and delivers it via two separate AAV vectors. Once in the cells, the two halves recombine to form the full-length protein. This dual vector technology is in advance stages of preclinical development for the treatment of USH1B.

UshTher, a multidisciplinary consortium of academic and industry partners, is a 5-year project supported by the Europe Commission. The objectives of UshTher are to produce dual AAV vectors for non-clinical studies, assess them in preclinical models, and conduct a multicenter, Phase I/II trial to investigate dual-AAV–based gene therapy for USH1B RP. The consortium is also conducting a natural history study. An initial pilot, preclinical safety and biodistribution study has been conducted in cynomolgus monkeys, and researchers from this consortium published data on a dual hybrid AAV vector serotype 8 (dual AAV8.h*MYO7A*), dose-ranging study in which non-human primates received a single subretinal injection that was well-tolerated and resulted in microscopic alterations. (UshTher 2021 [Web]; Ferla et al, 2021 [Congress presentation])

There are few details available concerning the agent in development by Atsena Therapeutics for USH1B, except the company notes it has developed dual AAV vectors capable of delivering the large genetic payload of *MYO7A*. (Atsena USH1B 2021 [Web])

Other Potentially Applicable Gene Therapies

BS01

Under development by Bionic Site, BS01 is a non-replicating rep/cap deleted recombinant adeno-associated virus vector expressing an

enhanced light-sensitive channelrhodopsin gene (ChronosFP) that is being studied in patients with RP who have bare light perception in ≥1 eye. The therapy targets the optic nerve and utilizes an optogenetic protein, which is then activated with a neural coding device. The device uses the retina's neural code to convert what individuals are viewing into signals the brain can understand. A report from the company in March 2021 noted BS01 showed biological activity in the first 4 trial participants treated, who were able to see light and motion. (NCT04278131 [Web]; Intrado 2021 [Press release]; Bionic Site 2021 [Web])

GS030

GS030 is an optogenetic gene therapy targeting retinal ganglion cells that encodes a light sensitive channelrhodopsin, *ChrimsonR-tdTomato*, delivered by an AAV2.7m8 vector and administered via intravitreal injection. It is utilized in conjunction with visual interface stimulating goggles that encode images of the visual world and modulate an amplifying light source projected onto the genetically engineered retina. The agent and device are being evaluated in the multicenter, open-label PIONEER trial. To date, 1 trial participant with a 40-year diagnosis of RP experienced partial recovery of vision, with the ability to perceive, locate, count, and touch different objects. (Martel et al, 2020 [Congress presentation]; Sahel et al, 2021)

MCO-010

Nanoscope Therapeutics' MCO-010 uses an intravitreally delivered proprietary AAV2 vector to deliver light sensitive multicharacteristic opsin (MCO) genes into retinal cells, where they express polychromatic opsins enabling vision in different color environments. A completed Phase I/IIa study demonstrated that MCO-010 was well-tolerated, with improved quality of life consistent with significant functional vision and visual function improvement in individuals with advanced RP. Nanoscope reported dosing of the first patient in the ongoing Phase IIb trial in July 2021. FDA has given MCO-010 orphan drug status. (Nanoscope 2021 [Web]; Hutton 2021 [News])

EYS611

EYS611 is a DNA plasmid that encodes for the human transferrin protein, which is an endogenous protein that helps manage iron levels in the eye. Iron overload has been associated with photoreceptor death in several retinal degenerative diseases. According to Eyevensys, by acting as an iron chelating and neuroprotective agent, EYS611 helps slow the progression of diseases like RP regardless of the specific genetic mutation causing the condition. The electrotransfection of EYS611 in the ciliary muscle delayed structural and functional degeneration in the Royal College of Surgeons (RSC) rat model of RP and decreased malondialdehyde (MDA) ocular content, a biomarker of oxidative stress. FDA has given EYS611 orphan drug status. (Eyevensys 2021 [Press release]; Bigot et al, 2020)

Cell-Based Therapies

hRPCs

ReNeuron's human retinal progenitor cell (hRPC) subretinal injection therapy is comprised of cells isolated from fetal retina that are capable of differentiating into components of the retina. The cells are used allogeneically (ie, cells from a single source are capable of treating multiple individuals) and are treatment agnostic to genetic subtype of disease. Results to date from a Phase I/IIa study in RP (n=22) showed generally well-tolerated dose escalation with no evidence of inflammation or proliferative vitreoretinopathy. However, there were 2 events resulting in vision loss related to surgical procedure or participant selection. (ReNeuron 2021 [Web]; Dugal 2019 [Congress presentation])

JCell

jCyte Inc., is also developing allogenic hRPC therapy given as an intravitreal injection for the treatment of RP. jCell's paracrine mechanism may result in significant slowing of host photoreceptor loss and is agnostic to genetic subtype. A Phase I/IIa dose escalation 12-month trial demonstrated a favorable safety profile and suggestion of treatment benefit. Results of the Phase IIb study in 84 participants demonstrated a

strong safety profile and encouraging biological activity, warranting progression to a phase 3 trial, according to the investigators. *Post hoc* analyses suggest the therapy could be more effective in a subgroup of patients defined by ellipsoid zone (EZ) or CFT thickness parameters. (Kuppermann et al, 2020 [Congress presentation]; Liao et al, 2021 [Congress presentation]; Srivastava et al, 2021[Congress presentation])

BMSC

As part of the open-label Stem Cell Ophthalmology Treatment Study (SCOTS), 5 individuals with USH were treated with autologous bone marrow derived stem cells (BMSC). Cells were isolated from the bone marrow using standard medical and surgical practices and administered into participants' eyes a combination of retrobulbar, sub-Tenon, intravitreal, subretinal, and intra-optic injections. Increases in visual acuity were noted in 80% of treated eyes. There was no reported visual loss nor any complications up to a year post-treatment (Weiss et al, 2019; French et al, 2020)

Other Therapies

NPI-001

Nacuity's N-acetylcysteine amide (NPI-001) is the amide form of N-acetylcysteine (NAC), an endogenous antioxidant moiety capable of facilitating glutathione (GSH) biosynthesis, replenishing GSH within cells that are undergoing oxidative stress. In mice models of RP, orally administered NAC reduced cone cell death and preserved cone function by reducing oxidative damage. In a phase I study in individuals with RP, NAC for 24 weeks resulted in significantly improved mean best corrected visual acuity (BCVA) and mean retinal sensitivity. NPI-001 is more lipophilic and more easily permeates cell membranes than NAC, and NPI-001 showed significantly greater preservation of cone cell function and cone survival compared with NAC in an *rd10+/+* mouse model. The Phase I/II SLO-RP study is being conducted in individuals with vision loss due to RP associated with USH. To be eligible, participants must be aged ≥18 years; have an EZ width ≥500 microns, which includes the fovea in each eye, at screening Visit 2; and ≥20 detectable points on the Macular Integrity

Assessment (MAIA) grid. (Nacuity 2021 [Web]; Sunitha et al, 2013; Lee et al, 2011; Campochiaro et al, 2020; Dong et al, 2014 [Congress presentation]; NCT04355689 [Web])

Citations

Adams B. Fierce Biotech. After 11 years, Sanofi kicks backs the rights to unwanted gene therapies to Oxford Biomedica. https://www.fiercebiotech.com/biotech/after-11-years-sanofi-kicks-backs-rights-to-unwanted-gene-therapies-to-oxford-biomedica. June 8, 2020. Accessed August 9, 2021.

Adato A, Weil D, Kalinski H, et al. Mutation profile of all 49 exons of the human myosin VIIA gene, and haplotype analysis, in Usher 1B families from diverse origins. *Am J Hum Genet*. 1997;61(4):813-821.

Atsena Therapeutics. Our programs. Pipeline. https://atsenatx.com/programs/pipeline/. Accessed August 9, 2021.

Atsena Therapeutics. Our programs. Usher syndrome 1B. https://atsenatx.com/programs/ush1b/. Accessed August 9, 2021.

Boëda B, El-Amraoui A, Bahloul A, et al. Myosin VIIa, harmonin and cadherin 23, three Usher I gene products that cooperate to shape the sensory hair cell bundle. *EMBO J*. 2002;21(24):6689-6699.

Bigot K, Gondouin P, Bénard R, Montagne P, Youale J, Piazza M, Picard E, Bordet T, Behar-Cohen F. Transferrin non-viral gene therapy for treatment of retinal degeneration. *Pharmaceutics*. 2020;12(9):836.

Bionic Site. Bionic Site Technology. https://www.bionicsightllc.com/technology. Accessed August 9, 2021.

Calabro KR, Boye SL, Choudhury S, et al. A novel mouse model of *MYO7A* USH1B reveals auditory and visual system haploinsufficiencies. *Front Neurosci*. 2019;13:1255.

Campochiaro PA, Iftikhar M, Hafiz G, et al. Oral N-acetylcysteine improves cone function in retinitis pigmentosa patients in phase I trial. *J Clin Invest*. 2020;130(3):1527-1541.

Colella P, Sommella A, Marrocco E, et al. Myosin7a deficiency results in reduced retinal activity which is improved by gene therapy. *PLoS One*. 2013;8(8):e72027.

de Joya EM, Colbert BM, Tang PC, et al. Usher syndrome in the inner ear: etiologies and advances in gene therapy. *Int J Mol Sci*. 2021;22(8):3910.

Derks MFL, Megens HJ, Giacomini WL, Groenen MAM, Lopes MS. A natural knockout of the MYO7A gene leads to pre-weaning mortality in pigs. *Anim Genet*. 2021;52(4):514-517.

Dong A, Stevens R, Hackett S, Campochiaro PA. Compared with N-acetylcysteine (NAC), N-acetylcysteine amide (NACA) provides increased protection of cone function in a model of retinitis pigmentosa. Presented at: The Association for Research in Vision Ophthalmology; May 4-8, 2014; Orlando, FL.

Dugal PU. Subretinal human retinal progenitor cells (hRPC) in retinitis pigmentosa (RP): A phase I/IIa updated. Presented at: The American Academy of Ophthalmology; October 12-15, 2019; San Francisco, CA.

Ernest S, Rauch GJ, Haffter P, Geisler R, Petit C, Nicolson T. Mariner is defective in myosin VIIA: a zebrafish model for human hereditary deafness. *Hum Mol Genet*. 2000;9(14):2189-2196.

Eyevensus. Eyevensys Receives FDA orphan drug designation for EYS611 for treatment of retinitis pigmentosa. https://www.eyevensys.com/eyevensys-receives-fda-orphan-drug-designation-for-eys611-for-treatment-of-retinitis-pigmentosa/. October 5, 2020. Accessed August 9, 2021.

Ferla R, Dell'Aquila F, Doria M, et al. Towards a clinical trial of gene therapy for retinitis pigmentosa associated with Usher syndrome type IB. Presented at: 24th Annual meeting of the American Society of Gene & Cell Therapy; May 11-14, 2021; Virtual.

Ferrari S, Di Iorio E, Barbaro V, Ponzin D, Sorrentino FS, Parmeggiani F. Retinitis pigmentosa: genes and disease mechanisms. *Curr Genomics*. 2011;12(4):238-249.

French LS, Mellough CB, Chen FK, Carvalho LS. A review of gene, drug and cell-based therapies for Usher Syndrome. *Front Cell Neurosci*. 2020;14:183.

Fuster-García C, García-Bohórquez B, Rodríguez-Muñoz A, Aller E, Jaijo T, Millán JM, García-García G. Usher Syndrome: Genetics of a Human Ciliopathy. *Int J Mol Sci*. 2021;22(13):6723.

Galbis-Martínez L, Blanco-Kelly F, García-García G, et al. Genotype-phenotype correlation in patients with Usher syndrome and pathogenic

variants in MYO7A: implications for future clinical trials. *Acta Ophthalmol*. 2021 Feb 11. doi: 10.1111/aos.14795. Epub ahead of print.

Gibbs D, Diemer T, Khanobdee K, Hu J, Bok D, Williams DS. Function of MYO7A in the human RPE and the validity of shaker1 mice as a model for Usher syndrome 1B. *Invest Ophthalmol Vis Sci*. 2010;51(2):1130-5.

Gibbs D, Kitamoto J, Williams DS. Abnormal phagocytosis by retinal pigmented epithelium that lacks myosin VIIa, the Usher syndrome 1B protein. *Proc Natl Acad Sci U S A*. 2003;100(11):6481-6486.

Gibson F, Walsh J, Mburu P, et al. A type VII myosin encoded by the mouse deafness gene shaker-1. *Nature*. 1995;374(6517):62-64.

Guzmán HO, Palacios AM, De Almada MI, Utrera RA. A novel homozygous MYO7A mutation involved in a Venezuelan population with high frequency of USHER1B. *Ophthalmic Genet*. 2016;37(3):328-330.

Hasson T, Heintzelman MB, Santos-Sacchi J, Corey DP, Mooseker MS. Expression in cochlea and retina of myosin VIIa, the gene product defective in Usher syndrome type 1B. *Proc Natl Acad Sci U S A*. 1995;92(21):9815-9819.

HGNC. Symbol report for MYO7A. https://www.genenames.org/data/gene-symbol-report/#!/hgnc_id/7606. Accessed August 4, 2021.

Hutton D. First patient dosed in optogenetic gene therapy trial. *Ophthalmology Times.* https://www.ophthalmologytimes.com/view/first-patient-dosed-in-optogenetic-gene-therapy-trial. July 19, 2021. Accessed August 9, 2021.

Intrado Globe Newswire. First four patients in bionic Sight's optogenetic gene therapy trial are able to detect light and motion. https://www.globenewswire.com/news-release/2021/03/30/2201412/0/en/First-Four-Patients-In-Bionic-Sight-s-Optogenetic-Gene-Therapy-Trial-Are-Able-To-Detect-Light-And-Motion.html. March 30, 2021. Accessed August 9, 2021.

Jacobson SG, Cideciyan AV, et al. Usher syndromes due to MYO7A, PCDH15, USH2A or GPR98 mutations share retinal disease mechanism. *Hum Mol Genet.* 2008;17(15):2405-2415.

Jacobson SG, Aleman TS, Sumaroka A, et al. Disease boundaries in the retina of patients with Usher syndrome caused by MYO7A gene mutations. *Invest Ophthalmol Vis Sci*. 2009;50(4):1886-1894.

Jacobson SG, Cideciyan AV, Gibbs D, et al. Retinal disease course in Usher syndrome 1B due to MYO7A mutations. *Invest Ophthalmol Vis Sci*. 2011;52(11):7924-7936.

Jaijo T, Aller E, Beneyto M, et al. MYO7A mutation screening in Usher syndrome type I patients from diverse origins. *J Med Genet*. 2007;44(3):e71.

Jaijo T, Aller E, Oltra S, et al. Mutation profile of the MYO7A gene in Spanish patients with Usher syndrome type I. *Hum Mutat*. 2006;27(3):290-291.

Jouret G, Poirsier C, Spodenkiewicz M, et al. Genetics of Usher syndrome: new insights from a meta-analysis. *Otol Neurotol*. 2019;40(1):121-129.

Khateb S, Mohand-Saïd S, Nassisi M, et al. Phenotypic characteristics of rod-cone dystrophy associated with MYO7A mutations in a large French cohort. *Retina*. 2020;40(8):1603-1615.

Keogh IJ, Godinho RN, Wu TP, et al. Clinical and genetic linkage analysis of a large Venezuelan kindred with Usher syndrome. *Int J Pediatr Otorhinolaryngol*. 2004;68(8):1063-1068.

Kimberling WJ, Hildebrand MS, Shearer AE, et al. Frequency of Usher syndrome in two pediatric populations: Implications for genetic screening of deaf and hard of hearing children. *Genet Med*. 2010;12(8):512-516.

Klomp AE, Teofilo K, Legacki E, Williams DS. Analysis of the linkage of MYRIP and MYO7A to melanosomes by RAB27A in retinal pigment epithelial cells. *Cell Motil Cytoskeleton*. 2007;64(6):474-487.

Koenekoop RK, Arriaga MA, Trzupek KM, Lentz JJ. Usher Syndrome Type I. 1999 Dec 10 [updated 2020 Oct 8]. In: Adam MP, Ardinger HH, Pagon RA, Wallace SE, Bean LJH, Mirzaa G, Amemiya A, editors. *GeneReviews*® [Internet]. Seattle (WA): University of Washington, Seattle; 1993–2021.

Kros CJ, Marcotti W, van Netten SM, et al. Reduced climbing and increased slipping adaptation in cochlear hair cells of mice with Myo7a mutations. *Nat Neurosci*. 2002;5(1):41-47.

Kuppa A, Sergeev YV. Homology modeling and global computational mutagenesis of human myosin VIIa. *J Anal Pharm Res*. 2021;10(1):41-48.

Kupperman BD. Intravitreal injection of allogeneic human retinal progenitor cells (jCell) for treatment of retinitis pigmentosa: results from the phase 2b trial. Presented at: Retina Society 2020 VR (53rd Annual Scientific Meeting).

Lee SY, Usui S, Zafar AB, Oveson BC, Jo YJ, Lu L, Masoudi S, Campochiaro PA. N-Acetylcysteine promotes long-term survival of cones in a model of retinitis pigmentosa. *J Cell Physiol*. 2011;226(7):1843-1849.

Lenassi E, Saihan Z, Cipriani V, et al. Natural history and retinal structure in patients with Usher syndrome type 1 owing to MYO7A mutation. *Ophthalmology*. 2014;121(2):580-587.

Li J, Chen Y, Deng Y, et al. Ca^{2+}-induced rigidity change of the myosin VIIa IQ motif-single α helix lever arm extension. *Structure*. 2017;25(4):579-591.e4.

Li S, Mecca A, Kim J, et al. Myosin-VIIa is expressed in multiple isoforms and essential for tensioning the hair cell mechanotransduction complex. *Nat Commun*. 2020;11(1):2066.

Liao D, Boyer DS, Kaiser P, et al. Intravitreal injection of allogeneic human retinal progenitor cells (hRPC) for treatment of retinitis pigmentosa: a prospective randomized controlled phase 2b trial. Presented at: The Association for Research in Vision Ophthalmology; May 1-7, 2021; Virtual.

Liu X, Ondek B, Williams DS. Mutant myosin VIIa causes defective melanosome distribution in the RPE of shaker-1 mice. *Nat Genet*. 1998;19(2):117-118.

Liu X, Udovichenko IP, Brown SD, Steel KP, Williams DS. Myosin VIIa participates in opsin transport through the photoreceptor cilium. *J Neurosci*. 1999;19(15):6267-6274.

Liu X, Vansant G, Udovichenko IP, Wolfrum U, Williams DS. Myosin VIIa, the product of the Usher 1B syndrome gene, is concentrated in the connecting cilia of photoreceptor cells. *Cell Motil Cytoskeleton*. 1997;37(3):240-252.

Lopes VS, Gibbs D, Libby RT, Aleman TS, Welch DL, Lillo C, Jacobson SG, Radu RA, Steel KP, Williams DS. The Usher 1B protein, MYO7A, is required for normal localization and function of the visual retinoid cycle enzyme, RPE65. *Hum Mol Genet*. 2011;20(13):2560-2570.

Lopes VS, Ramalho JS, Owen DM, Karl MO, Strauss O, Futter CE, Seabra MC. The ternary Rab27a-Myrip-Myosin VIIa complex regulates

melanosome motility in the retinal pigment epithelium. *Traffic*. 2007;8(5):486-499.

Lopes VS, Williams DS. Gene therapy for the retinal degeneration of Usher syndrome caused by mutations in MYO7A. *Cold Spring Harb Perspect Med*. 2015;5(6):a017319.

Lu Y, Zhou D, King R, et al. The genetic dissection of *Myo7a* gene expression in the retinas of BXD mice. *Mol Vis*. 2018;24:115-126.

Martel J, Degli Esposti S, Boulanger-Scemama E, et al. Optogenetics in the clinic: PIONEER, a phase 1/2a gene therapy program for non-syndromic retinitis pigmentosa. Presented at: The Association for Research in Vision Ophthalmology; May 3-7, 2020; Virtual.

Mburu P, Liu XZ, Walsh J, et al. Mutation analysis of the mouse myosin VIIA deafness gene. *Genes Funct*. 1997;1(3):191-203.

Millán JM, Aller E, Jaijo T, Blanco-Kelly F, Gimenez-Pardo A, Ayuso C. An update on the genetics of usher syndrome. *J Ophthalmol*. 2011;2011:417217.

Miller KA, Williams LH, Rose E, Kuiper M, Dahl HH, Manji SS. Inner ear morphology is perturbed in two novel mouse models of recessive deafness. *PLoS One*. 2012;7(12):e51284.

Mohand-Said S, Azoulay-Sebban L, Audo IS, et al. Natural history of retinal function and structure in a French cohort of patients with Usher syndrome Type 1 due to *MYO7A* mutations. Presented at: The Association for Research in Vision Ophthalmology; May 7-11, 2017; Baltimore, MD.

Mohand-Said S, Boelle P-Y, Nassibi N, et al. natural history of retinal function and structure in a French cohort of patients with Usher syndrome. Presented at: The Association for Research in Vision Ophthalmology; April 29-May 3, 2018; Honolulu, HI.

Nacuity Pharmaceuticals, Inc. Our science. https://www.nacuity.com/our-science/. Accessed August 9, 2021.

Nanoscope Therapeutics. Our pipeline. https://nanostherapeutics.com/pipeline/. Accessed August 9, 2021.

NCBI. MYO7A myosin VIIA [*Homo sapiens* (human)]. https://www.ncbi.nlm.nih.gov/gene/4647. Updated August 2, 2021. Accessed August 4, 2021.

NCT01505062. Study of SAR421869 in participants with retinitis pigmentosa associated with Usher syndrome type 1B. https://clinicaltrials.gov/ct2/show/study/NCT01505062?term=NCT01505062&draw=2&rank=1. Updated March 18, 2020. Accessed August 9, 2021.

NCT02065011. A study to determine the long-term safety, tolerability and biological activity of SAR421869 in patients with Usher syndrome type 1B. https://clinicaltrials.gov/ct2/show/NCT02065011?term=SAR421869&draw=2&rank=2. Updated August 11, 2020. Accessed August 9, 2021.

NCT02320812. Safety of a single, intravitreal injection of human retinal progenitor cells (jCell) in retinitis pigmentosa. https://clinicaltrials.gov/ct2/show/NCT02320812?term=jcyte&draw=2&rank=3. Updated March 5, 2019. Accessed August 9, 2021.

NCT02464436. Safety and Tolerability of hRPC in Retinitis Pigmentosa (hRPCRP). https://clinicaltrials.gov/ct2/show/NCT02464436?term=ReNeuron&draw=2&rank=2. Updated August 3, 2021. Accessed August 9, 2021.

NCT02556736. RST-001 Phase I/II trial for advanced retinitis pigmentosa. https://clinicaltrials.gov/ct2/show/NCT02556736?term=NCT02556736&draw=2&rank=1. Updated June 23, 2021. Accessed August 9, 2021.

NCT03011541. Stem cell ophthalmology treatment study II (SCOTS2). https://clinicaltrials.gov/ct2/show/NCT03011541?term=NCT03011541&draw=2&rank=1. Updated February 24, 2021. Accessed August 9, 2021.

NCT03073733. Safety and efficacy of intravitreal injection of human retinal progenitor cells in adults with retinitis pigmentosa. https://clinicaltrials.gov/ct2/show/NCT03073733?term=jcyte&draw=2&rank=2. Updated May 6, 2021. Accessed August 9, 2021.

NCT04278131. BS01 in patients with retinitis pigmentosa. https://clinicaltrials.gov/ct2/show/NCT04278131?term=NCT04278131&draw=2&rank=1. Updated July 27, 2021. Accessed August 9, 2021.

NCT04355689. Safety and efficacy of NPI-001 tablets for RP associated with Usher syndrome (SLO RP). https://clinicaltrials.gov/ct2/show/NCT04355689?term=NCT04355689&draw=2&rank=1. Updated June 28, 2021. Accessed August 9, 2021.

NCT04604899. Safety of repeat intravitreal injection of human retinal progenitor cells (jCell) in adult subjects with retinitis pigmentosa.

https://clinicaltrials.gov/ct2/show/NCT04604899?term=jcyte&draw=2&rank=1. Updated May 7, 2021. Accessed August 9, 2021.

NCT04919473. Dose-escalation study to evaluate the safety and tolerability of intravitreal vMCO-I in patients with advanced retinitis pigmentosa. https://clinicaltrials.gov/ct2/show/NCT04919473?term=NCT04919473&draw=2&rank=1. Updated June 9, 2021. Accessed August 9, 2021.

NCT04945772. Efficacy and safety of vMCO-010 optogenetic therapy in adults with retinitis pigmentosa [RESTORE] (RESTORE). https://clinicaltrials.gov/ct2/show/NCT04945772?term=NCT04945772&draw=2&rank=1. Updated July 30, 2021. Accessed August 9, 2021.

Novartis AG. Novartis acquires Vedere Bio, adding novel optogenetic gene therapy technology for treating blindness. https://www.novartis.com/news/media-releases/novartis-acquires-vedere-bio-adding-novel-optogenetic-gene-therapy-technology-treating-blindness. October 29, 2020. Accessed August 25, 2021.

OMIM. *276903 MYOSIN VIIA; MYO7A. https://www.omim.org/entry/276903#geneMap. Updated December 23, 2019. Accessed August 4, 2021.

Peng YW, Zallocchi M, Wang WM, Delimont D, Cosgrove D. Moderate light-induced degeneration of rod photoreceptors with delayed transducin translocation in shaker1 mice. *Invest Ophthalmol Vis Sci*. 2011;52(9):6421-6427.

ReNeuron. Our products & technologies. http://www.reneuron.com/products/products-technologies/#products. Accessed August 9, 2021.

Rhodes CR, Hertzano R, Fuchs H, et al. A Myo7a mutation cosegregates with stereocilia defects and low-frequency hearing impairment. *Mamm Genome*. 2004;15(9):686-697.

Sahel JA, Boulanger-Scemama E, Pagot C, et al. Partial recovery of visual function in a blind patient after optogenetic therapy. *Nat Med*. 2021;27(7):1223-1229.

Sahly I, Dufour E, Schietroma C, et al. Localization of Usher 1 proteins to the photoreceptor calyceal processes, which are absent from mice. *J Cell Biol*. 2012;199(2):381-399.

Sakai T, Jung HS, Sato O, et al. Structure and regulation of the movement of human myosin VIIA. *J Biol Chem*. 2015;290(28):17587-17598.

Sato O, Komatsu S, Sakai T, et al. Human myosin VIIa is a very slow processive motor protein on various cellular actin structures. *J Biol Chem*. 2017 Jun 30;292(26):10950-10960.

Schwander M, Lopes V, Sczaniecka A, et al. A novel allele of myosin VIIa reveals a critical function for the C-terminal FERM domain for melanosome transport in retinal pigment epithelial cells. *J Neurosci*. 2009;29(50):15810-15818.

Schwander M, Sczaniecka A, Grillet N, et al. A forward genetics screen in mice identifies recessive deafness traits and reveals that pejvakin is essential for outer hair cell function. *J Neurosci*. 2007;27(9):2163-2175.

Self T, Mahony M, Fleming J, Walsh J, Brown SD, Steel KP. Shaker-1 mutations reveal roles for myosin VIIA in both development and function of cochlear hair cells. *Development*. 1998;125(4):557-566.

Small L, Wong J, Pennesi ME, et al. Multimodal imaging in patients with MYO7A-related Usher syndrome. Presented at: The Association for Research in Vision Ophthalmology; May 3-7, 2020; Virtual.

Srivastava S, Kaiser PK, Kammer R, et al. Predictive relationship of OCT characteristics for efficacy in an intravitreal injection of allogeneic human retinal progenitor cells (hRPC) for the treatment of retinitis pigmentosa. Presented at: The Association for Research in Vision Ophthalmology; May 1-7, 2021; Virtual.

Stephenson K, Dockery A, Wynne NC, et al. The phenotype & genotype of Usher syndrome in Ireland. Presented at: The Association for Research in Vision Ophthalmology; April 28-May 2, 2019; Vancouver, Canada.

Subirà O, Català-Mora J, Díaz-Cascajosa J, et al. Retinal findings in pediatric patients with Usher syndrome Type 1 due to mutations in MYO7A gene. *Eye (Lond)*. 2020;34(3):499-506.

Sumaroka A, Matsui R, Cideciyan AV, et al. Outer retinal changes including the ellipsoid zone band in Usher syndrome 1B due to MYO7A mutations. *Invest Ophthalmol Vis Sci*. 2016;57(9):OCT253-61.

Sunitha K, Hemshekhar M, Thushara RM, et al. N-Acetylcysteine amide: a derivative to fulfill the promises of N-Acetylcysteine. *Free Radic Res*. 2013;47(5):357-367.

Testa F, Carreno E, Vermeer K, et al. Baseline characteristics of patients with Usher syndrome due to *MYO7A* mutations enrolled in a prospective natural history study. Presented at: The Association for Research in Vision Ophthalmology; May 3-7, 2020; Virtual.

Testa F, Melillo P, Bonnet C, et al. Clinical presentation and disease course of Usher syndrome because of mutations in MYO7A or USH2A. *Retina*. 2017;37(8):1581-1590.

Toms M, Pagarkar W, Moosajee M. Usher syndrome: clinical features, molecular genetics and advancing therapeutics. *Ther Adv Ophthalmol*. 2020;12:2515841420952194.

Trapani I, Auricchio A. Has retinal gene therapy come of age? From bench to bedside and back to bench. *Hum Mol Genet*. 2019;28(R1):R108-R118.

UnitProt. UniProtKB - Q13402 (MYO7A_HUMAN). https://www.uniprot.org/uniprot/Q13402. Updated June 2, 2021. Accessed August 4, 2021.

UshTher. Periodic Reporting for period 2 - UshTher (Clinical trial of gene therapy with dual AAV vectors for retinitis pigmentosa in patients with Usher syndrome type IB). https://cordis.europa.eu/project/id/754848/reporting. Updated September 2, 2021. Accessed September 7, 2021.

Wasfy MM, Matsui JI, Miller J, Dowling JE, Perkins BD. myosin 7aa(-/-) mutant zebrafish show mild photoreceptor degeneration and reduced electroretinographic responses. *Exp Eye Res*. 2014;122:65-76.

Watanabe S, Umeki N, Ikebe R, Ikebe M. Impacts of Usher syndrome type IB mutations on human myosin VIIa motor function. *Biochemistry*. 2008;47(36):9505-9513.

Weil D, Blanchard S, Kaplan J, et al. Defective myosin VIIA gene responsible for Usher syndrome type 1B. *Nature*. 1995;374(6517):60-61.

Weil D, Levy G, Sahly I, et al. Human myosin VIIA responsible for the Usher 1B syndrome: a predicted membrane-associated motor protein expressed in developing sensory epithelia. *Proc Natl Acad Sci U S A*. 1996;93(8):3232-3237.

Weiss JN, Levy S. Stem Cell Ophthalmology Treatment Study (SCOTS): bone marrow derived stem cells in the treatment of Usher syndrome. *Stem Cell Investig*. 2019;6:31.

Williams DS. Usher syndrome: animal models, retinal function of Usher proteins, and prospects for gene therapy. *Vision Res*. 2008;48(3):433-441.

Williams DS, Lopes VS. The many different cellular functions of MYO7A in the retina. *Biochem Soc Trans*. 2011;39(5):1207-1210.

Zallocchi M, Binley K, Lad Y, et al. EIAV-based retinal gene therapy in the shaker1 mouse model for usher syndrome type 1B: development of UshStat. *PLoS One*. 2014;9(4):e94272.